Combining Electro-Fenton and adsorption processes for reclamation of textile industry wastewater and modeling by Artificial neural Networks

Ayşe Kuleyin, Aysem Gök, Handan Atalay, Feryal Akbal, Amane Jada, Joelle Duplay

Combining Electro-Fenton and adsorption processes for reclamation of textile industry wastewater and modeling by Artificial neural Networks

Ayşe Kuleyin [a], Ayşem Gök [a], Handan Atalay Eroğlu [a], E. Burcu Özkaraova [a], Feryal Akbal [a,⇑], Amane Jada [b], Joelle Duply [c]

[a] *Ondokuz Mayıs University, Environmental Engineering Department, Kurupelit-Samsun, Türkiye*

[b] *Institute of Materials Science, Mulhouse, France*

[c] *Earth and Environment Institute of Strasbourg, Strasbourg, France*

ABSTRACT

In the present study, coupling electro-Fenton (EF) and adsorption processes for textile industry wastewater remediation was investigated, in both batch and continuous flow modes. Sepiolite was used as an adsorbent in the coupled EF/adsorption processes. Various parameters such as reaction time, current intensity, Fe^{2+} con- centration, sepiolite dose, and flow rate were found to affect the efficiency of the coupled processes. In com- parison to the single EF process, a synergistic effect occurred in the coupled EF/adsorption processes, leading to better performance for COD and TOC removal from textile wastewater. Thus, in the single EF technology, using graphite felt electrodes, COD and TOC removal efficiencies from real textile wastewater, were 58 % and 36 %, respectively. However, in the coupled EF/adsorption processes, COD and TOC removal efficiencies increased to 85 % and to 63 %, respectively. The higher COD and TOC removals may be attributed to the combined effect of adsorption and oxidation reactions in coupled EF/adsorption process. Moreover, Artificial Neural Networks (ANN) model was built up in order to estimate COD and TOC removal efficiencies of the coupled EF/adsorption processes. A good correlation was found between the ANN model theoretical prediction, and the experimental data, for COD and TOC removals, in both batch and continuous modes. The novelty of the current work lies in the synergistic effect occurring between the EF and adsorption processes in wastewater treatment and provides the ANN model as a valuable tool for describing COD and TOC removal efficiencies under different experimen- tal conditions.

1. Introduction

Textile industries consume great amounts of water and auxiliary chemicals in the finishing and dyeing operations and produce large volumes of wastewater containing various dyes and process chemicals [1]. The resulting textile industry wastewaters represent the high colour, turbidity, chemical oxygen demand (COD), biochemical oxygen demand (BOD), pH values, inorganic salts, and toxic substance amounts [2]. The discharge of textile effluents into aquatic media can cause serious environmental damages, due to their intense colour, high organic load and low biodegradability. Therefore, textile effluents need to be treated to meet discharge standards in accordance with the relevant regulations. Various techniques, such as conventional physicochemical and biological processes are employed for textile wastewaters treatment [3]. However, conventional treatment methods generally result in low decolourization and organic matter degradation, and they are not efficient for the reclamation of textile wastewaters [4]. Advanced treatment techniques, such as activated carbon adsorption [5], membrane processes [6], advanced oxidation processes (AOPs) [7] and electrochemical processes [8] have been integrated with the conventional treatment methods for the reclamation of textile wastewaters.

Recently electrochemical advanced oxidation processes (EAOPs) have received great attention for the treatment of wastewaters containing recalcitrant organic contaminants owing to their high efficiency, cost-effectiveness and environmental compatibility [9]. EAOPs can be classified as direct and indirect EAOPs according to the production mechanism of hydroxyl radicals ($OH^{\bullet}$). In direct EAOPs the $OH^{\bullet}$ are produced at the anode surface by direct oxidation of water while in indirect EAOPs, $OH^{\bullet}$ are produced by the in situ formed or externally added chemicals [10]. Anodic oxidation (AO) is based on the oxidation of organic pollutants by the direct electron transfer

and heterogeneous $OH^{\bullet}$ produced at the anode. The efficiency of the AO process depends on the selection of anode material. The anodes used in the AO process are classified as active and non-active anodes. Active anodes, such as Pt, IrO_2, RuO_2 and graphite, have high electrocatalytic activity and chemical stability. However, they produce chemisorbed $OH^{\bullet}$ which are less available and only allow the partial oxidation of organic contaminants due to their low oxygen evolution overpotential. Non-active anodes such as PbO_2, BDD, and SnO_2 possess a high oxygen evolution overpotential and produce physically adsorbed $OH^{\bullet}$, which are not strongly attached to the electrode and are more available for oxidation reactions. Therefore, organic contaminants are oxidized efficiently, since $OH^{\bullet}$ are formed in high amounts and can react readily with organic contaminants [11]. In the AO process, contaminant degradation occurs through the conversion of organic contaminants into biodegradable by-products such as short-chain carboxylic acids, and the complete decomposition of organic contaminants into CO_2, H_2O and inorganic ions [12].

Among the electrochemical AOPs (EAOPs), the EF process has been proven as the most effective technology to achieve fast and complete degradation of organic contaminants in water [13]. In the EF process, the electrolysis continuously generates H_2O_2 in solution by the cathodic reduction of oxygen in the acid medium (Eq. (1)). Electrochemical production of H_2O_2 from oxygen is an attractive and sustainable method for in situ H_2O_2 production under ambient conditions [14–18]. The addition of ferrous ions into the solution leads to the generation of $OH^{\bullet}$ by Fenton's reaction (Eq. (2)). The $OH^{\bullet}$ are highly reactive oxidizing agents and non-selectively attack organic contaminants leading to their complete decomposition [19]. In the EF process, the Fe^{2+} ions are also regenerated by the following reactions. (Eq. (3–7)) [12]. Heterogeneous hydroxyl radical ($M(OH^{\bullet})$) is also produced at the anode (Eq. (8)) in addition to homogeneously produced $OH^{\bullet}$ in the solution. The $M(OH^{\bullet})$ contributes significantly to the decomposition and mineralization of organics in the EF processes [20]. In the EF process, carbonaceous materials are widely used as the cathode, owing to their broad electrochemical activity for O_2 reduction and low catalytic activity for H_2O_2 decomposition. Also, carbonaceous materials like carbon felt and graphite felt have a high porosity which is beneficial for absorbing oxygen gas supplied near the cathode and resulting in the formation of a higher amount of hydrogen peroxide [12].

$$O_2 + 2H^{+} + 2e^{-} \rightarrow H_2O_2 \quad (1)$$

$$Fe^{2+} + H_2O_2 \rightarrow Fe^{3+} + OH^{-} + OH^{\bullet} \quad (2)$$

$$Fe^{3+} + H_2O \rightarrow Fe(OH)^{2+} + H^{+} \quad (3)$$

$$Fe(OH)^{2+} + e^{-} \rightarrow Fe^{2+} + OH^{-} \quad (4)$$

$$Fe^{3+} + H_2O_2 \rightarrow Fe^{2+} + H^{+} + HO_2^{\bullet} \quad (5)$$

$$Fe^{3+} + HO_2^{\bullet} \rightarrow Fe^{2+} + H^{+} + O_2 \quad (6)$$

$$Fe^{3+} + R^{\bullet} \rightarrow Fe^{2+} + R^{+} \quad (7)$$

$$M + H_2O \rightarrow M(OH^{\bullet}) + H^{+} + e^{-} \quad (8)$$

EF oxidation represents a promising alternative to classical Fenton oxidation for the treatment of wastewaters. In the EF process, organic contaminants in wastewater are oxidized either by abstraction of H^{+} ion or by addition of $OH^{\bullet}$ to multiple bonds and intermediate radical species (hydroxylation). As a result of consecutive oxidation steps, short-chain organic acids (e.g., oxalic acid) are produced which are relatively stable towards further oxidation by $OH^{\bullet}$, particularly in the presence of Fe^{3+} ions. Finally, complete mineralization of pollutants is achieved [21]. Compared with the classical Fenton process, the electro-Fenton process is advantageous in terms of better control of the process and preventing the storage and transport of H_2O_2 [22]. Furthermore, electricity used in the EF process is a clean energy source, therefore the overall process is accepted not to cause secondary pollution. EF process is regarded as an environment-friendly method in water and wastewater treatment since it doesn't use any harmful reagents [23]. EF process can be integrated with the biological treatment as a pre-treatment or post-treatment process. EF pre-treatment is applied to enhance the biodegradability of wastewater while EF post-treatment is applied as a polishing step of treated wastewaters to remove refractory organics.

Adsorption is considered one of the most prevailing processes for dyes removal and is widely used for the decolourization of industrial wastewaters. In the adsorption process, the selection of adsorbents is crucial and many types of adsorbents have been used in wastewater treatment. Among the adsorbents, clay minerals have been increasingly receiving attention because of their low cost, sheet-like structures, and high specific surface area. Sepiolite which constitutes an important group of clay minerals is a naturally hydrated magnesium silicate ($(Si_{12})(Mg_8)O_{30}(OH_6).(OH_2)_4{\cdot}8H_2O$). Structurally, it consists of blocks and channels extending in the fiber direction [24]. A great number of silanol (Si–OH) groups exist on the external surface of sepiolite which are accessible to organic species, acting as neutral adsorption sites [25]. Sepiolite has been used as an adsorbent in the removal of dyes and has been found to have a high adsorption capacity for both anionic and cationic dyes [26]. Although the adsorption process is effective in removing both organic and inorganic pollutants, it generates wastes that should be disposed of properly to reduce environmental risks. The regeneration of adsorbents is of great interest to reduce the waste generated in adsorption and the economic cost of wastewater treatment. Various techniques based on chemical, biological and physical processes are used for the regeneration of spent adsorbents. EAOPs can be a promising method for regenerating spent adsorbents due to the formation of highly reactive species that can oxidize a wide variety of pollutants [27].

The novelty of this study is the coupling of the electro-Fenton and adsorption processes to enhance the removal of refractory organics from biologically treated textile industry wastewater and to improve the treated wastewater quality. The combination of the electro-Fenton and adsorption process enables the removal of organic pollutants through both oxidation and adsorption as well as regeneration of the adsorbent during the electro-Fenton process. The coupled EF/adsorption method was applied in batch and continuous mode using graphite felt electrodes for the reclamation of textile industry wastewater. Batch experiments were performed at different oxidation times, currents, Fe^{2+} concentrations and sepiolite doses in order to obtain optimal operating conditions. Continuous experiments were also performed at different flow rates to assess the practical applicability of the EF process. The feasibility of coupled EF/adsorption process was additionally evaluated in terms of energy consumption. ANN modeling was used to predict the performance of the EF/adsorption process.

2. Materials and methods

2.1. Materials

$FeSO_4{\cdot}7H_2O$, H_2SO_4, and $Ca(OH)_2$ were of analytical grade and supplied from Merck and Sigma-Aldrich. All solutions were prepared with ultrapure water. Graphite felt was obtained from Mersen, Türkiye.

2.2. Textile wastewater

The textile wastewater samples used in this study were taken from a textile factory located at Çorlu in Türkiye. The main wastewater

sources in the textile industry are synthetic yarn and fabric production and dying operations. The wastewater samples used in the experiments were collected from the outlet line of the biological treatment unit. The suspended particles in the wastewater were removed by sand filtration before performing the experimental studies. Table 1 shows the characteristics of textile wastewater.

2.3. Experimental system

The experimental studies were conducted in batch and continuous modes of operation. The experiments were performed in an undivided electrochemical reactor with a volume of 0.5 L for the batch system and 1.5 L for the continuous system equipped with graphite felt electrodes (Fig. 1). The dimensions of the electrodes were 4.5 × 6 × 0.3 cm for the batch reactor and 8 × 10 × 0.3 cm for the continuous reactor. The electrodes were placed into the EF reactor with an interval of 4 cm. The pH of wastewater was adjusted to pH 3.0 before starting the EF experiments by using a pH meter (Thermo Scientific Orion Star A215). The pH of the solution was not controlled during the reaction. Experiments were conducted with the natural conductivity of textile wastewater. The wastewater was stirred with a magnetic stirrer at a rate of 250 rpm to provide complete mixing conditions in all experiments. The voltage was supplied by a DC power supply (GE). $FeSO_4$ was used as the catalyst in EF experiments. In the coupled EF/adsorption experiments, sepiolite was added to the EF reactor as a low-cost adsorbent. Continuous aeration was performed by using air diffusers submerged in both reactors. At the end of EF and EF/adsorption experiments, the pH of samples was adjusted between 7 and 9 to stop the oxidation process. Before the analysis, all samples were filtered by 0.45 um PTFE filters. In the batch experiments, the influence of Fe^{2+} concentration (1–3 mM), applied current (0.35–0.55 A) and reaction time (0–60 min) was examined while in the continuous experiments the influence of flow rates (25 and 50 mL min^{-1}) was investigated.

2.4. Analytical methods

Textile wastewater characterization before and after experiments was performed in terms of pH, electrical conductivity, colour, COD and total organic carbon (TOC) according to standard methods. The colour (Pt-Co) was measured by Hach-Lange spectrophotometer (DR6000).COD analyses were carried out by means of the standard closed reflux method using a Hach-Lange spectrophotometer (DR6000).TOC was determined through the combustion of the sample at 700℃ using a TOC analyzer with NDIR detector (Teledyne Tekmar Lotix). TOC standard solution was used to check the measurements.

The colour, COD and TOC removal percentage was calculated by:

$$Colour(\%) = \left(\frac{C_0 - C_t}{C_0}\right) \times 100 \quad (9)$$

$$COD(\%) = \left(\frac{COD_0 - COD_t}{COD_0}\right) \times 100 \quad (10)$$

$$TOC(\%) = \left(\frac{TOC_0 - TOC_t}{TOC_0}\right) \times 100 \quad (11)$$

where C_0 is the initial and C_t is the final colour, COD and TOC concentrations of textile wastewater.

Table 1
Characteristics of textile wastewater.

Parameter	Unit	Range	Average
pH	–	7.4–8.4	7.97
EC	(μS/cm)	2380–4000	3034
Colour	(Pt-Co)	150–210	184
COD	(mg/L)	91–98	95
TOC	(mg/L)	23–32	28
Chloride	(mg/L)	93–633	356
Sulfate	(mg/L)	35–418	236
RES 436 nm	(m^{-1})	4.90–6.50	5.63
RES 525 nm	(m^{-1})	3.30–4.70	4.12
RES 620 nm	(m^{-1})	1.85–2.90	2.43

2.5. Characterization of sepiolite

Sepiolite used in this study was obtained from Eskişehir (Türkiye). It was crushed with a mechanic mill and was sieved to obtain a fraction between 0.425 and 0.600 mm). The XRD spectrum of the sepiolite sample was recorded by using an X-ray diffractometer operating in transmission geometry (STOE Stadi-P diffractometer, IS2M, Mulhouse-France). The XRD scan was performed at 40 kV and 40 mA, in the range of 5° < 2θ < 80° at a step size of 0.02° and a scan rate of 0.3 s/step, by using a monochromatic radiation λ(KαCu) = 1,5418 Å.

The elemental composition of the sample was performed by energy-dispersive X-ray spectroscopy (EDX, Quanta 400, IS2M, Mulhouse-France). Brunauer, Emmett-Teller specific surface area (BET, ASAP 2020 V4.00 IS2M, Mulhouse-France) was used to determine the specific surface area and the pore volume of sepiolite. Scanning Electron Microscopy analyses were performed by using SEM (Quanta 400, IS2M, Mulhouse-France) with a maximum voltage of 20 V.

2.6. Energy consumption

Economic feasibility of the EF and EF/adsorption system was evaluated with regard to electrical energy consumption (EEC) which was calculated as in Eq. (12):

$$EEC\ (kwh\,g^{-1}COD) = \frac{E_{cell} I \Delta t}{(COD_0 - COD_t) V} \quad (12)$$

where E_{cell} is the average cell voltage (V), I is the applied current (A), Δt is the electrolysis time (h), V is the volume of wastewater (L), and COD_0 and COD_t are the COD values (mg L^{-1}) at initial and specified electrolysis time [28].

2.7. Artificial neural network modelling

Artificial neural network (ANN) was employed to predict the treatment efficiency of the EF/adsorption process in batch and continuous systems. ANN calculations were performed using Matlab R 2020b software. The three-layered feed forward back propagation neural network was used for modeling of EF/adsorption process. The input variables were applied current (A), electrolysis time (min), Fe^{2+} concentration (mM) and sepiolite dose (g L^{-1}) in the batch system and flow rate (ml min^{-1}), time (min) and sepiolite addition in the continuous system. COD and TOC removals were selected as the output variables. In total, 176 of the experimental dataset including 96 batch and 80 continuous system data were used to develop the ANN model. The dataset was randomly divided into training, validation and test sets with a ratio of 70 %, 15 % and 15 %.

3. Results and discussion

3.1. Sepiolite characterization

3.1.1. XRD analysis

Characterization of sepiolite by XRD revealed that it contained 68.147 % of SiO_2, 27.420 % of MgO, 3.514 % of CaO and minor amounts of Na_2O, K_2O, NiO, Fe_2O_3, Al_2O_3, SO_3, Cr_2O_3. As expected, the sepiolite is magnesium phyllosilicate.

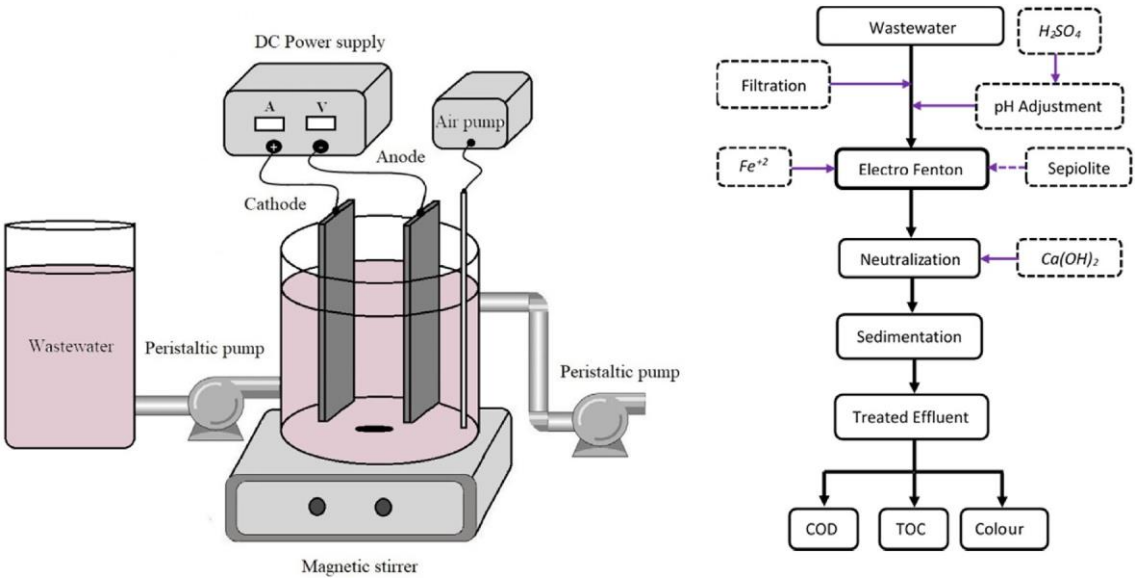

Fig. 1. Schematic diagram of EF reactor and experimental methodology.

3.1.2. N_2 adsorption/desorption analysis

Fig. 2(a) shows the N_2 adsorption/desorption isotherms using the BET analysis (ASAP 2020 V4.00 (V4.00*H*), IS2M). Fig. 2(b) shows the BET plot of the Nitrogen adsorption on sepiolite from which the specific surface area was determined. Fig. 2(c) shows the determined BJH pore size distribution of the sepiolite. As can be seen in Fig. 2 (a) the N_2 adsorption–desorption isotherms of the sepiolite sample are of type IV with hysteresis loops, mostly attributed to mesoporous materials, according to IUPAC classification. From Fig. 2(b) the calculated specific surface area is 329.7 m^2/g. From Fig. 2(c) and by using the BJH method, the pore volume and the average pore diameter of the sepiolite were calculated as, respectively, 0.486 $cm^3\ g^{-1}$ and 17.2 nm. The higher values of the sepiolite's specific surface area and pore volume account for its use as an adsorbent for wastewater treatment and result from the configuration of the sepiolite fiber, consisting of elongated hollow bricks.

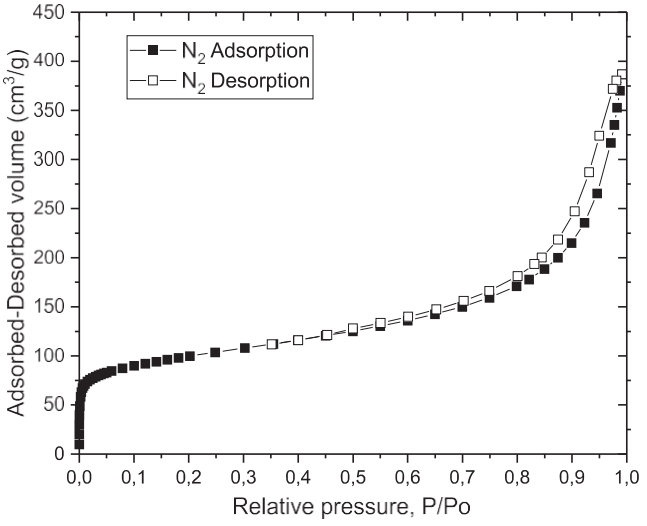

Fig. 2. (a). N_2 adsorption–desorption isotherms of Sepiolite (b). BET plot of the Nitrogen adsorption on sepiolite (c) BJH pore size distribution of Sepiolite (d). SEM image of sepiolite (e). EDX spectrum of sepiolite (f). XRD spectrum of sepiolite.

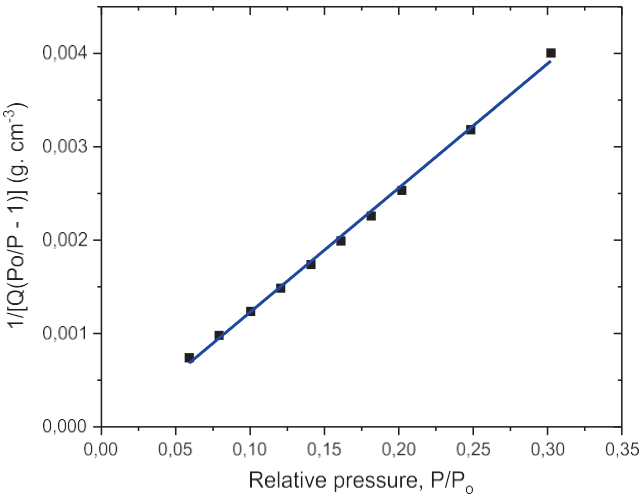

Fig. 2 (*continued*)

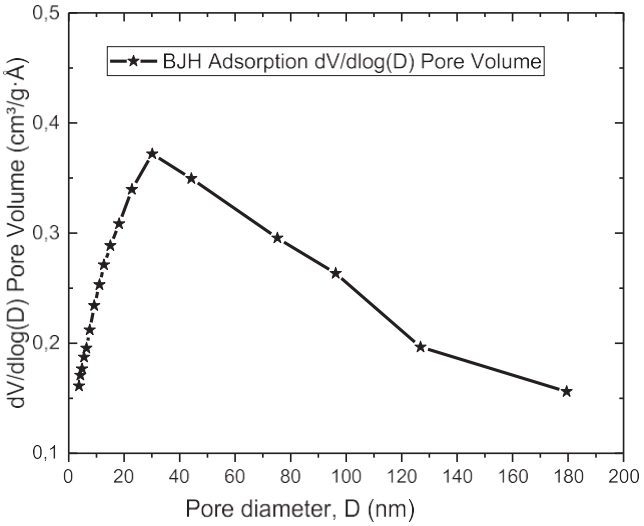

Fig. 2 (*continued*)

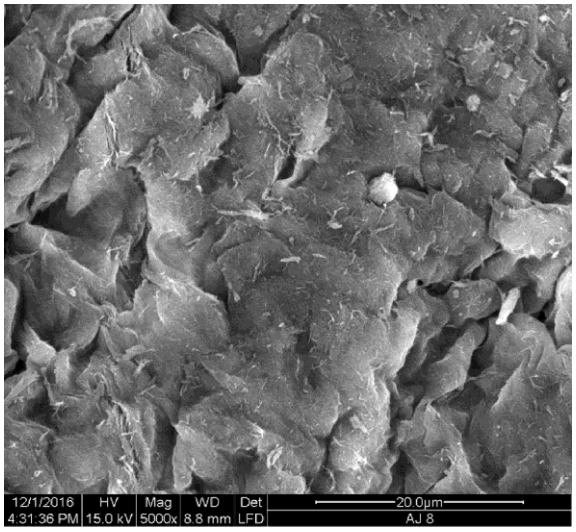

Fig. 2 (*continued*)

3.1.3. SEM and EDX analyses

Fig. 2(d) shows the SEM images and Fig. 2(e) shows the EDX spectrum of sepiolite. As can be seen in this figure, the EDX spectrum shows three main peaks due to the presence of Mg, Si, and O, in good agreement with the XRD analysis, whereas from the SEM images, the micro-fibrous form of sepiolite is clearly evidenced.

3.1.4. XRD analyses

The XRD pattern of the purified sepiolite is shown in Fig. 2(f). As can be seen in this figure, the sepiolite characteristic peaks occurring at 2θ = 7.1°, 11.7°, 13.1°, 17.7°, 19.7°, 20.6°, 28.2°, 29.5°, 34.6° and 39.5° are comparable to those contained in Sepiolite JCPDS card (No. 75-1597). Further, thanks to Bragg's law (2dsinθ = nλ), the intense peak centered at 2θ = 7.15° is attributed to the layer spacing d_{110} = 1.24 nm of the sepiolite. In addition, Fig. 2(f), shows reflections at 2θ = 20.7° and 37.6° which correspond to the quartz characteristic reflections whereas the reflections occurring at 2θ = 29.4° and 36.5° are attributed to the carbonates impurities. The overall X-ray data of the sepiolite as presented in Fig. 2 (f) are in good agreement with the sepiolite crystalline properties found in the literature.

3.2. Batch Electro-Fenton process

3.2.1. Effect of applied current

The applied current is one of the main operating parameters influencing the performance of the electro-Fenton process, as it promotes the production of $OH^{\bullet}$ (Eq. (2)) by means of the electrochemical generation of H_2O_2 in the solution (Eq. (1)) and the regeneration of Fe^{2+} from Fe^{3+} (Eq. (3–7)) and also the generation of $OH^{\bullet}$ at the anode surface (Eq. (8)). In order to determine the optimum current, experiments were performed at current values in the range of 0.35 A and 0.75 A (6.5–13 mA cm^{-2}) in the presence of 2 mM Fe^{2+} with and without sepiolite. Fig. 3(a) shows the colour removal by single EF and coupled EF/adsorption processes, at different current values. It can be seen from the figure that colour removal by EF and coupled EF/adsorption processes were almost same and the effect of current on colour removal was insignificant. The influence of current on the COD removal was shown in Fig. 3(b). As can be seen, the higher removal percentages of COD were reached at higher currents in EF and coupled EF/adsorption process. The COD removal efficiencies were 80 %, 85 % and 94 % for the EF/adsorption process and 36.5 %, 58 % and 62.4 % for the EF process at applied currents of 0.35, 0.55, 0.75A, respectively. Regarding the increase in COD removal efficiency observed

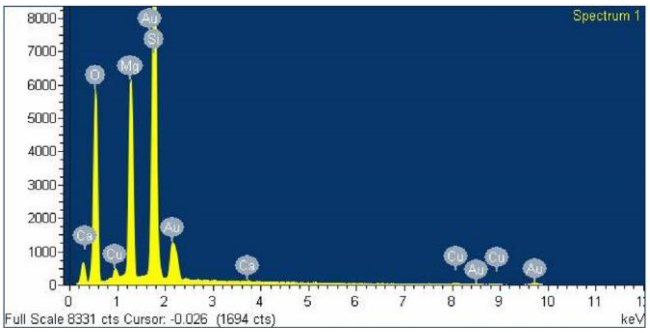

Fig. 2 (*continued*)

for the EF process and the potential variations in textile wastewater composition [29], 0.55 A (10 $mAcm^{-2}$) was selected as the optimum current for the subsequent experiments. The increased oxidation rate at a higher current could be attributed to the increased rate of H_2O_2 formation (Eq. (1)) as well as the faster regeneration of Fe^{2+} (Eq. (3–7)), resulting in the generation of higher amounts of $OH^{\bullet}$ by Fenton's reaction (Eq. (2)). Similar results were reported by Panizza and Oturan [30], for the oxidation of Alizarin Red dye by the EF process using graphite felt cathode. Li et al. [31] investigated the production of H_2O_2 at different voltages for graphite felt electrodes. They reported that as the voltage increases, the current density increases and this leads to an increase in the H_2O_2 production efficiency.

On the other hand, TOC removal slightly increased when the applied current increased (Fig. 3(c)). TOC concentrations were reduced by 62.5 %, 63 % and 63.6 % in EF/adsorption process and 32.3 %, 36 % and 42.3 % for EF process at 0.35 A, 0.55 A and 0.75 A, respectively. Panizza and Cerisola [32] investigated the electrochemical oxidation of anthraquinone dye Alizarin Red by using a gas diffusion cathode and reported that the COD removal rate increased gradually with increasing current from 100 to 200 mA. Similarly, Rego et al. [33] investigated the degradation of Novacron Blue dye by the EF process and stated that the increase in applied current resulted in an increase in COD removal. The higher COD removals at higher currents were associated with higher H_2O_2 production and consequently greater $OH^{\bullet}$ generation. The colour, COD and TOC removal rates are relatively fast at the initial stage of EF oxidation for ≤15 min. However, it was observed that the removal rate decreased with longer oxidation times due to the formation of carboxylic acids by the oxidation

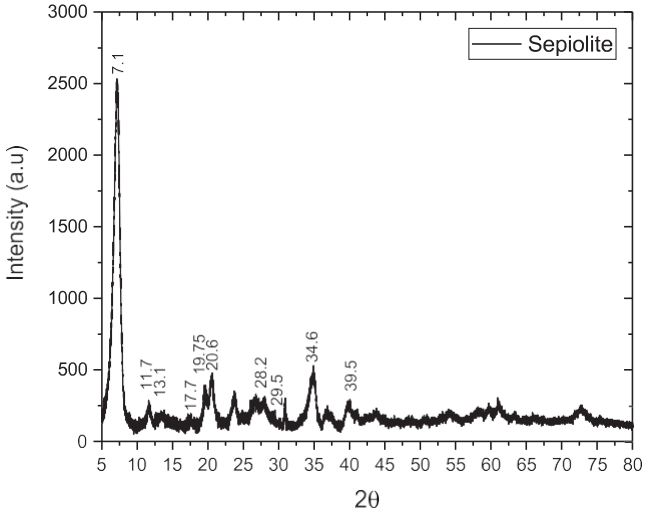

Fig. 2 (*continued*)

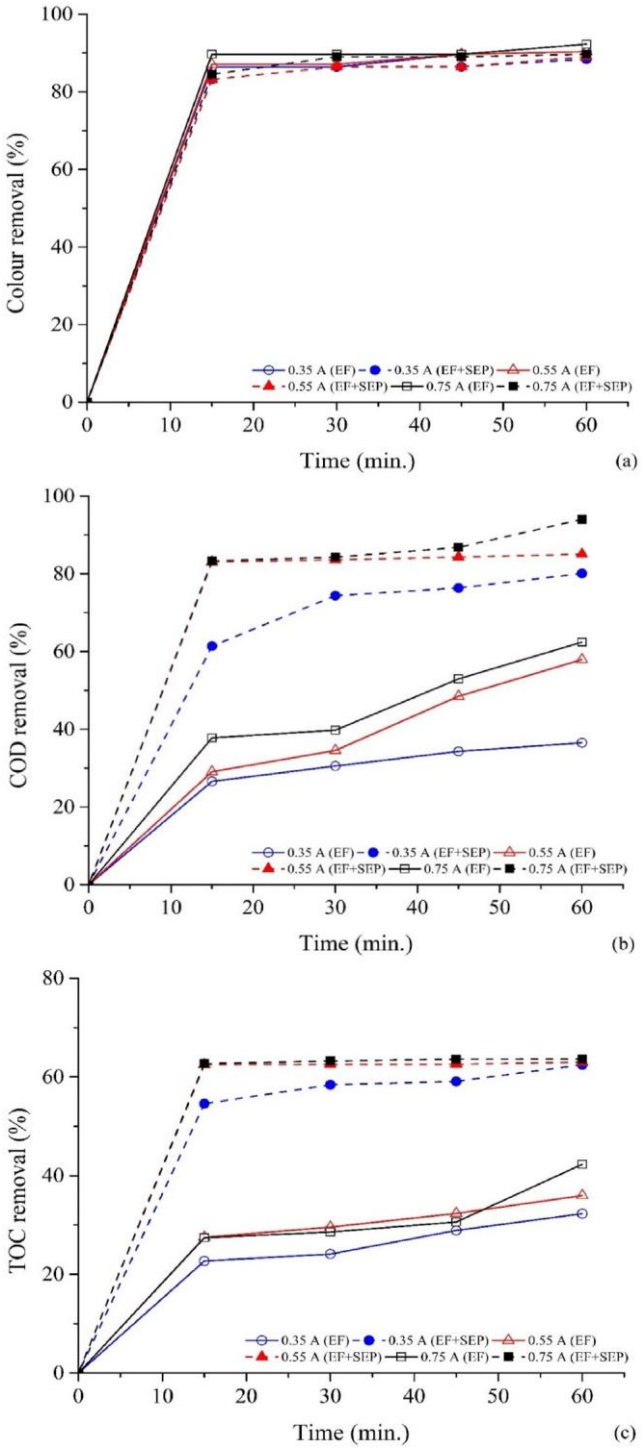

Fig. 3. Effects of time and current on (a) colour, (b) COD and (c) TOC removal by EF and EF/adsorption processes.

reactions which are less reactive towards $OH^{\bullet}$ when compared to parent compounds [34].

Energy consumption is a principal factor to evaluate the feasibility of the EF process in wastewater treatment. Energy consumption of EF and EF/adsorption process for different applied currents were shown in Fig. 4. It can be seen that the increase in the applied current resulted in higher EEC. In the EF process, energy consumptions were 0.19 kWh g^{-1} COD for 0.35 A and 0.45 kwh g^{-1} COD for 0.75 A. The increase in energy consumption by the applied current indicates that more energy

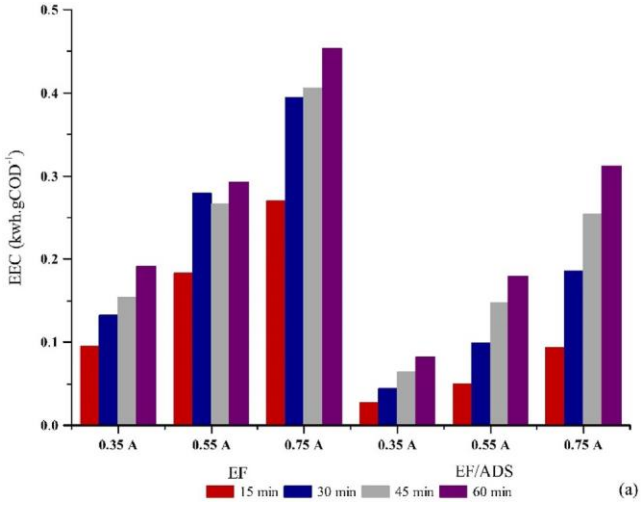

Fig. 4. Energy consumption of EF and EF/adsorption processes at different currents.

was spent for side reactions at higher currents. In EF/adsorption process lower energy consumptions were obtained than that of the EF process, 0.08 kWh g^{-1} COD for 0.35 A and 0.31 kWh g^{-1} COD for 0.75 A.

3.2.2. *Effect of Fe concentration*

The concentration of Fe^{2+} which is employed as the catalyst is one of the important parameters influencing the efficiency of the EF process. Fe^{2+} concentration determines the amounts of $OH^{\bullet}$ production, according to Eq. (2). The efficiency of the EF process increases with Fe^{2+} concentration, since the concentration of $OH^{\bullet}$, which are the main oxidizing agents in the EF process, increase with increasing Fe^{2+} concentration. However, when the ferrous ions present in the wastewater are in excess amounts, degradation rates reduce due to the consumption of $OH^{\bullet}$ [23]. The high concentrations of Fe^{2+} also cause the formation of iron precipitates, decreasing the current efficiency. Therefore, the optimal Fe^{2+} concentration should be determined to maximize the efficiency of the EF process [35].

The experiments were performed to investigate the effect of different Fe^{2+} concentrations on the colour, COD and TOC removals. The colour removal at different Fe^{2+} concentrations was shown in Fig. 5 (a). As can be seen, colour removal was almost same for all the Fe^{2+} concentrations. On the other hand, Fe^{2+}concentration has been observed to significantly affect COD removal (Fig. 5 (b)). The COD removal efficiencies were 54 %, 58 % and 70.7 % for EF and 78.8 %, 85 % and 92.6 % for EF/adsorption process at Fe^{2+} concentrations of 1, 2 and 3 mM, respectively. Similarly, TOC removal increased for EF and EF/ adsorption process with the increased Fe^{2+} concentration. The TOC removal efficiencies were 33 %, 36 % and 47.7 % for EF and 45 %, 63 % and 67 % for EF/adsorption process at Fe^{2+} concentrations of 1, 2 and 3 mM, respectively (Fig. 5(c)). This can be ascribed to the increased rate of $OH^{\bullet}$ production with increasing Fe^{2+}concentration, resulting in improved removal efficiencies.

The removal of COD and TOC increased with the increasing electrolysis time. The rate of removal was found to be very high in the early stage of the EF process (about 15 min) for overall Fe^{2+} concentrations. In the initial stage of electrolysis, Fe^{2+} ions which are in high concentrations in wastewater react with the H_2O_2 produced at the cathode to generate $OH^{\bullet}$. The Fe^{2+}concentration decreases with electrolysis time because of the formation of iron hydroxides as well as adsorption on the cathode surface resulting in a decrease in the EF process efficiency [36].

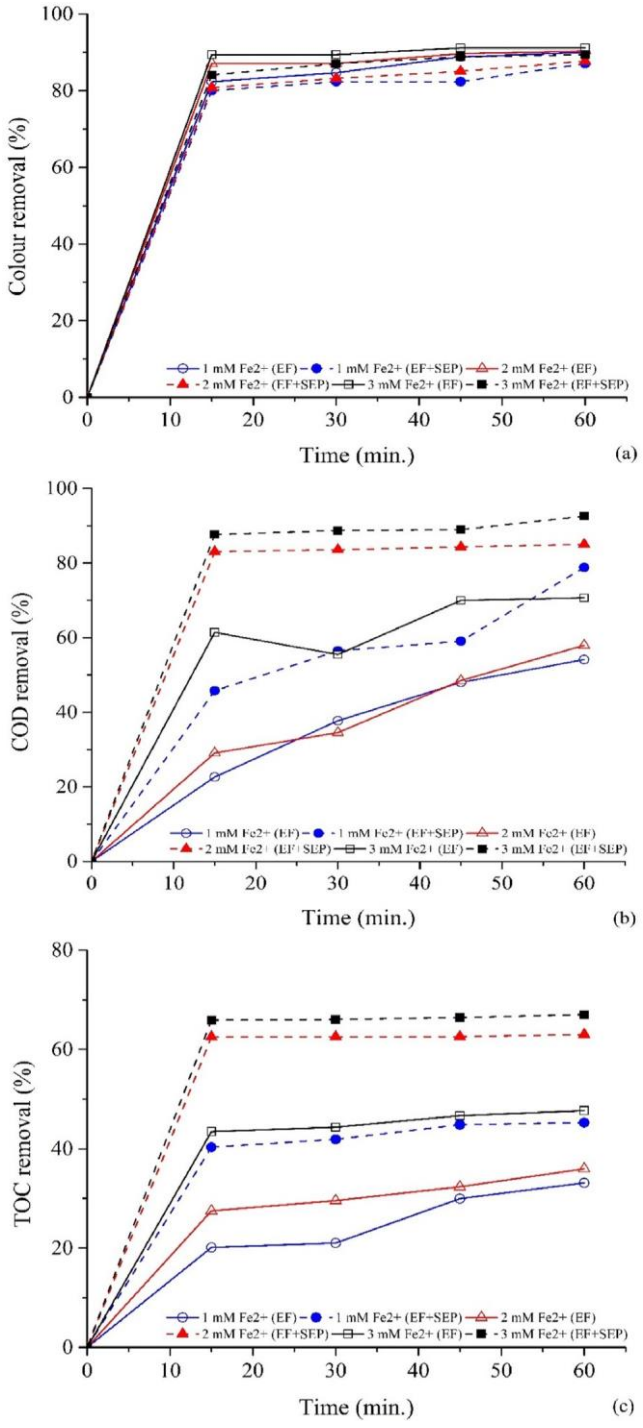

Fig. 5. Effects of time and Fe^{2+} concentration on (a) colour, (b) COD and (c) TOC removals by EF and EF/adsorption processes.

Previous studies have shown that the oxidation efficiency increased as the Fe^{2+} concentration increased. Wang et al. [37] reported that COD removal efficiency from real dyeing wastewater increased from 19.8 % to 43.1 % with the addition of Fe^{2+} at a concentration of 0.33 mM and the maximum COD removal of 75.2 % was achieved with a Fe^{2+} concentration of 2 mM. El-Desoky et al. [34] reported that a 30 % colour removal of Ponceau S azo-dye was attained with an EF treatment for 210 min in the absence of Fe^{2+} ions. The colour removal increased with increasing Fe^{2+} concentration up to 0.1 mM and then decreased due to the scavenging effect of Fe^{2+} ions on the $OH^{\bullet}$ formed. The complete colour removal of Ponceau S was attained by EF treatment for 150, 45, 90 and 180 min in presence of 0.05, 0.1, 0.5 and 1.0 mM $FeSO_4$, respectively.

Fig. 6 shows the energy consumptions for different Fe^{2+} concentrations. It can be seen that the energy consumption reduced with increasing Fe^{2+} concentration in the EF process. The energy consumption was obtained as 0.39 and 0.23 kWh g^{-1} COD for Fe^{2+} concentrations of 1 mM and 3 mM, respectively. In EF/adsorption process, energy consumption reduced from 0.25 to 0.18 kWh g^{-1} COD by increasing Fe^{2+} concentration from 1 mM to 2 mM, then gradually increased to 0.26 kWh g^{-1} COD at 3 mM Fe^{2+} concentration. Minimum energy consumption was obtained at 0.55 A, 2 mM Fe^{2+}, 5 g/L sepiolite dose and 60 min in EF/adsorption process. Considering the colour, COD and TOC removal efficiencies and energy consumption, the optimum Fe^{2+} concentration was determined as 2 mM.

3.3. Effect of sepiolite dose

In the EF/adsorption process, the influence of sepiolite dose on the removal of colour, COD and TOC was investigated, using different sepiolite doses ranging from 2.5 to 10.0 g/L. As can be seen from Fig. 7, the colour removal efficiency didn't change significantly with increasing sepiolite dose. On the other hand, an increase was observed in COD removal from 78.5 to 91 % and TOC removal from 54.4 % to 68.3 % when the sepiolite dose increased from 2.5 to 10 g/L at 60 min EF/adsorption treatment. Whereas COD and TOC removals were 57.9 % and 35.9 % after 60 min of EF treatment in the absence of sepiolite under the same experimental conditions. The increase in COD and TOC removal with increasing sepiolite dose may be attributed to the increase of surface area for the adsorption of organic pollutants.

3.4. Comparison of processes

To evaluate the advantage of the coupled EF/adsorption process, comparative studies between EF/adsorption, EF and adsorption processes were conducted under optimum experimental conditions (Fe^{2+} concentration of 2 mM, applied current of 0.55 A, and sepiolite dose 5 g/L). Adsorption experiments were performed in the same reactor without the use of chemicals and electrolysis. The colour, COD and TOC removal efficiencies of EF/adsorption, EF and adsorption processes are shown in Fig. 8. It can be seen that the colour removal by adsorption is very low compared to the other processes. After 60 min, while the colour removal efficiency was 49 % with adsorption,

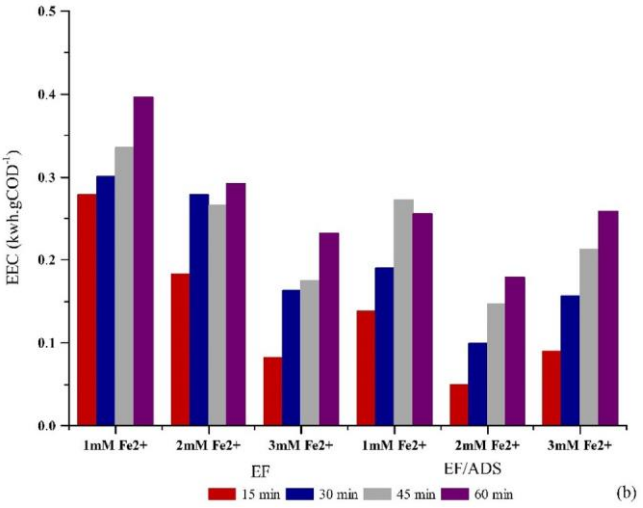

Fig. 6. Energy consumption of EF and EF/adsorption processes at different Fe^{2+} concentrations.

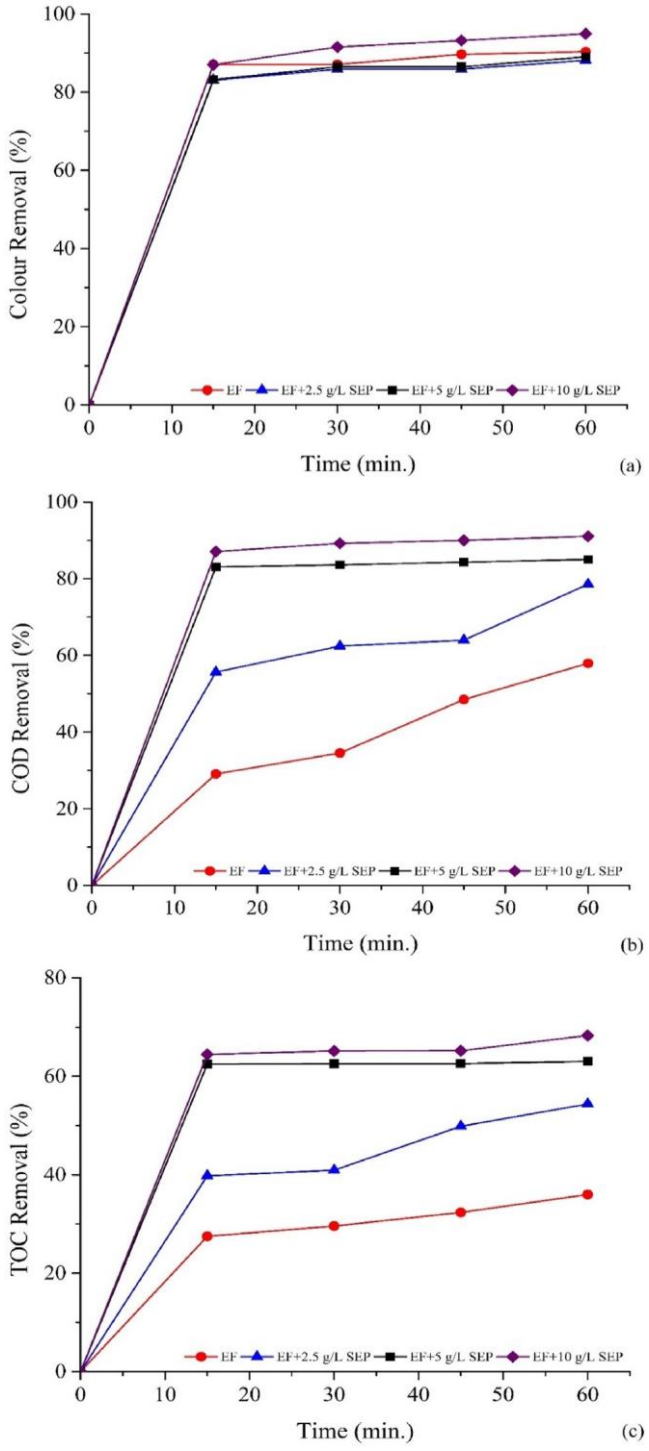

Fig. 7. Effects of time and sepiolite dose on (a) colour, (b) COD and (c) TOC removals by EF/adsorption processes.

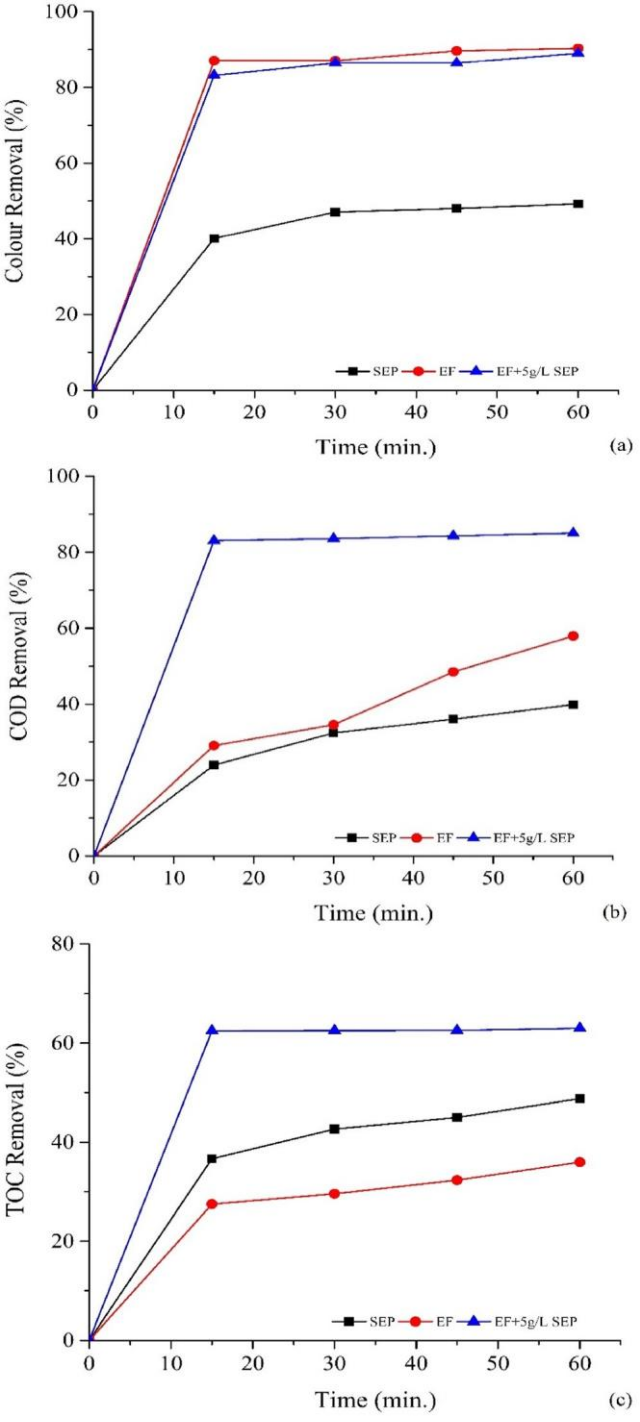

Fig. 8. Comparison of EF, adsorption and EF/adsorption processes for (a) colour, (b) COD and (c) TOC removals.

90 % colour removal was obtained with EF and EF/adsorption processes (Fig. 8(a)).

The COD removal was greater in the EF/adsorption process when compared with the classical EF and adsorption processes (Fig. 8(b)). After 60 min, the COD was reduced by 85 % by EF/adsorption, 58 % by the classic EF, and 40 % by the adsorption process. The TOC removal efficiency by the EF/adsorption process was about 63 % after 60 min, which was higher than that of the EF (36 %) and adsorption processes (49 %) (Fig. 8(c)). Integration of EF and adsorption process was found to improve the COD and TOC removal efficiencies compared to the single processes, which may be attributed to the combined effect of adsorption and oxidation processes [38].

The degradation mechanism of organic pollutants may be explained by the direct oxidation on the anode surface and the indirect oxidation by $OH^{\bullet}$ produced in the EF reaction. The graphite felt used in this study is an active anode (low O_2 evolution overpotential), therefore it is thought that heterogeneous $OH^{\bullet}$ produced at the anode surface may cause partial oxidation of organic pollutants. On the other hand, homogenous $OH^{\bullet}$ produced through the reaction of

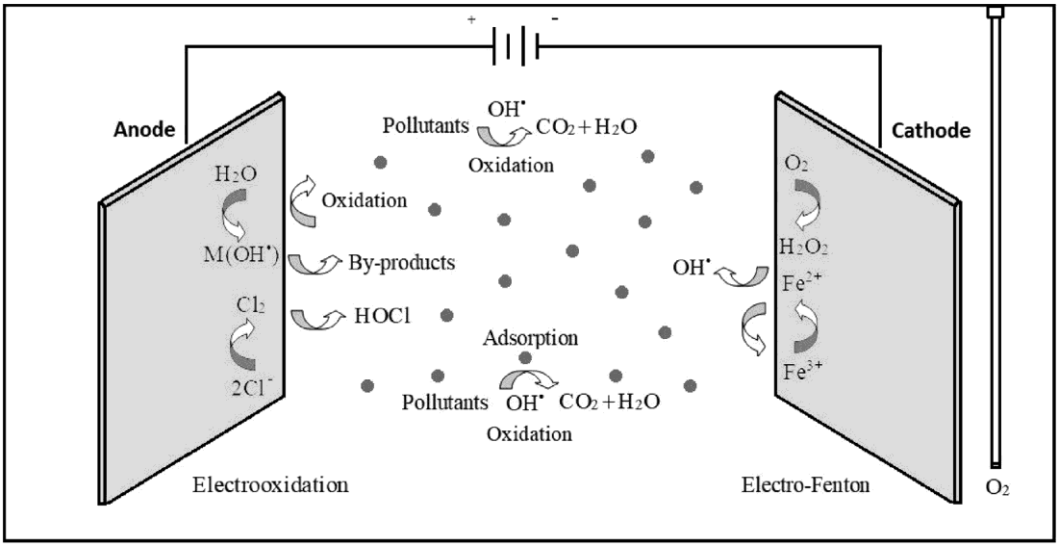

Fig. 9. Degradation mechanism of organic pollutants in EF/ADS system.

electrogenerated H_2O_2 and externally added Fe^{2+} ions in the EF process has a significant role in the oxidation of organic pollutants. In the EF/adsorption process, the $OH^{\bullet}$ in the solution also reacts with the adsorbed pollutants achieving the regeneration of the adsorbent. In the coupled EF/adsorption process, removal of pollutants by adsorption and regeneration of the adsorbent by EF oxidation occur simultaneously resulting in enhanced treatment efficiency. Furthermore, competitive reactions may occur on the anode surface and in the aqueous phase during electrochemical oxidation, since textile wastewater contains inorganic ions such as chloride and sulfate [39]. The chloride ions in the textile wastewater produce reactive chlorine species by electrochemical reactions which contribute to the oxidation of organic pollutants [13]. Chloride ions are oxidized to produce chlorine which is then transformed into hypochlorous acid and hypochlorite ions by hydrolysis reaction (Eq. (13–15)) [10]. At pH values < 5, the hypochlorous acid is the dominant form and may increase

Table 2
Literature on the treatment of real industrial textile effluents by electrochemical processes.

Wastewater type	Initial COD mg/L	Process	Operating conditions	Electrode type	%COD removal	%TOC removal	%Colour removal	Ref.
Biologically Treated textile ww	91–98	E-Fenton + Adsorption	10 mA/cm^2, pH 3.0, 1 mM Fe^{2+}, 60 min, 5 g/L sepiolite dose	Graphite felt electrodes	58	36	90	Present study
Biologically Treated textile ww	91–98	E-Fenton	10 mA/cm^2 pH 3.0, 1 mM Fe^{2+} 60 min	Graphite felt electrodes	85	63	90	Present study
Real Textile ww	262	EC + E-Fenton	10 mA/cm^2 EF pH 3, 60 min	EC (Fe/Fe)+EF (BDD/CF)	98.5	98.10	100	[8]
Real dyeing ww	1224	E-Fenton	3.2 mA/cm^2 pH 3, 240 min, 2 mM Fe^{2+}	Activated carbon fiber cathode, platinum wire anode	75.20			[37]
Real Textile ww	2154	Electrochemical oxidation	60 mA/cm^2, 3.0 g/L NaCl, pH 2.0, 3 h	Bipolar boron-doped diamond electrodes	100	–	–	[40]
Real Textile ww (Acrylic)	347	Electrochemical oxidation	27.8 A/m^2, 2.0 g/L NaCl pH 4.0, 110 min	Graphite electrodes	90.78	–	96.27	[41]
Real Textile ww	530	Electrochemical oxidation	45 A/m^2, pH 7.9	Graphite electrodes	93.00	–	–	[42]
Treated textile ww	704	SZVI-assisted Electro-oxidation (EO/SZVI)	20 mA/cm^2, pH 3.5, 30 min	Scrap zero-valent iron (SZVI) anode and graphite cathode	67.00	59.00	100.00	[43]
Printing and dyeing mill ww	443	Electrochemical oxidation	50 A/m^2, 0.2 g NaCl, pH 7.0, 20 min	Expanded graphite/ attapulgite anode and copper cathode	43.50	–	90.60	[44]
Real Textile ww	325	EC + E-Fenton	10 mA/cm^2, pH 3, 60 min	Iron electrode	95.00	99.00	96.00	[45]
Real Textile ww	1310	E-Fenton	4.76 mA/cm^2, pH 3, 160 min	Platinum sheet anode-Graphite felt cathode	64.20	–	77.00	[46]
Real Textile ww	1310	E-Chemical Fenton	4.76 mA/cm^2, pH 3, 40 min, 500 mg/L H_2O_2	Iron electrode	82.10	–	94.40	[46]
Real Textile ww	1698	E-Fenton	10 mA/cm^2, pH 3 0.3 mM Fe^{2+}	BDD anode and Ti cathode,	52.00	45.00	95.00	[47]
Real Textile ww	300	E-Fenton	0.45 mA/cm^2, 180 min	Carbon fiber cathode and a stainless-steel mesh anode	55.00		85.00	[48]

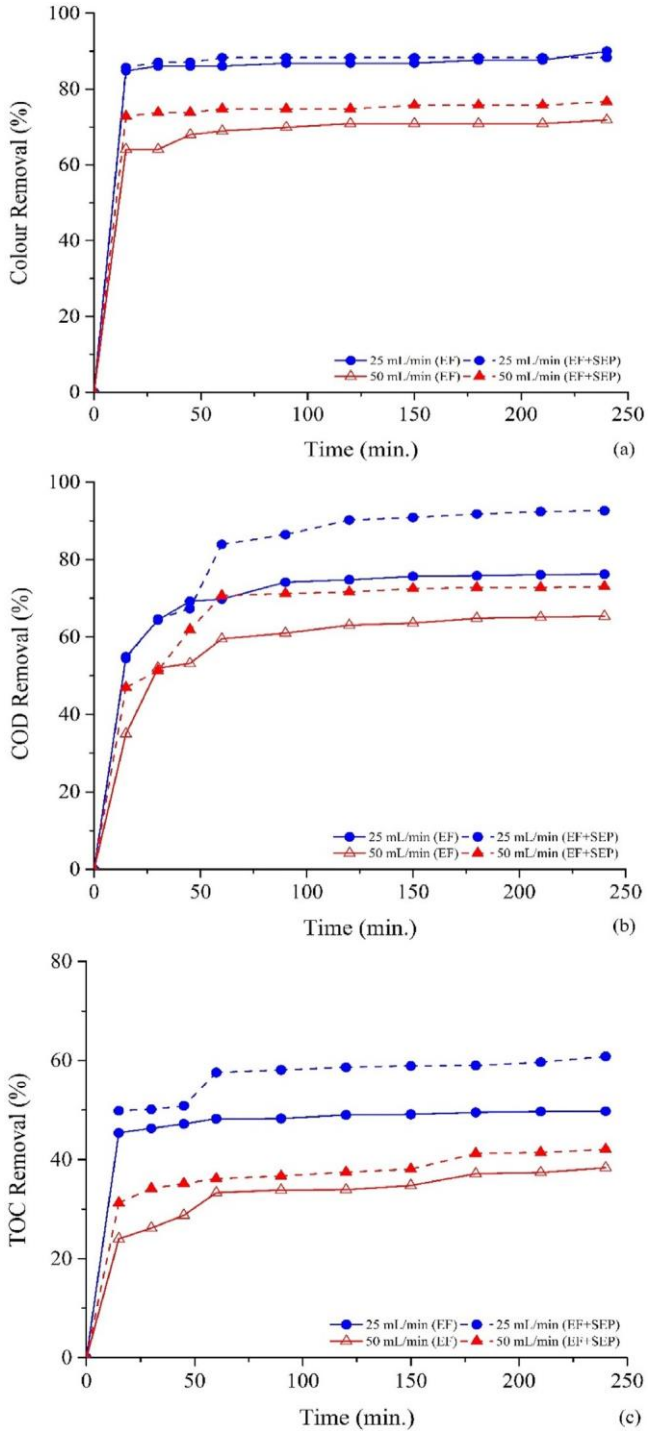

Fig. 10. Effects of time and flow rate on (a) colour, (b) COD and (c) TOC removals in continuous EF and EF/adsorption processes.

the performance of EF treatment. The proposed degradation mechanism of organic pollutants in textile wastewater by the EF/adsorption system is shown in Fig. 9.

$$2Cl^- \rightleftharpoons Cl_2 + 2e^- \quad (13)$$

$$Cl_2 + H_2O \rightleftharpoons HOCl + Cl^- + H^+ \quad (14)$$

$$HOCl \rightleftharpoons H^+ + OCl^- \quad (15)$$

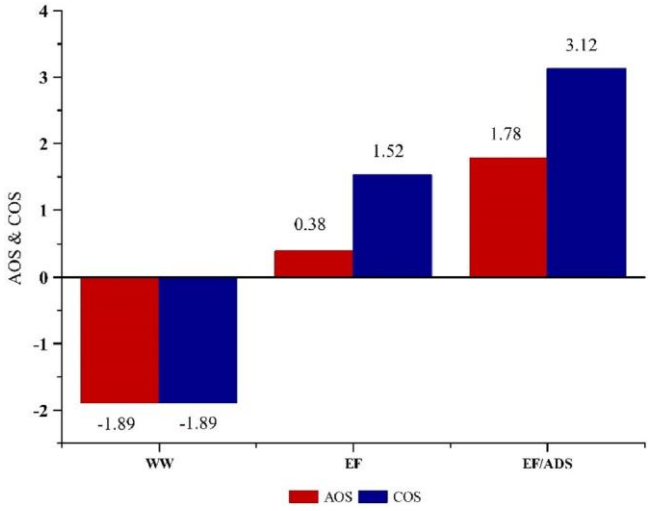

Fig. 11. AOS and COS values before and after EF and EF/adsorption treatment of textile wastewater.

Several researchers have investigated the feasibility of electrochemical oxidation of textile wastewater with various electrode materials such as titanium-based electrodes, platinum electrodes, diamond and metal alloy electrodes, boron-doped diamond electrodes, carbon fiber, and graphite felt electrodes. The comparison of the results obtained in this study with the results of previous researches on textile wastewater treatment by EF oxidation is given in Table 2.

3.5. Continuous Electro-Fenton process

EF and EF/adsorption reactors were operated in continuous mode for the up-scaling of the system. The optimal parameters obtained from batch experiments (Fe^{2+} concentration of 1 mM, applied current of 0.55 A (current density of 10 $mAcm^{-2}$), sepiolite dose of 5 g/L, and wastewater pH of 3) were applied for the continuous flow experiments. The wastewater flow rate was set at 25 mL min^{-1} and 50 mL min^{-1} to maintain the HRT at 30 min and 60 min. The reactor was stirred at a rate of 250 rpm to ensure the complete mixing of the wastewater.

Fig. 10(a) shows the influence of flow rate on the colour removal efficiency. The higher colour removals were reached with the lower flow rates but there was no significant difference between the EF and EF/adsorption processes. Fig. 10(b) presents the COD removal efficiencies for different flow rates. The higher COD removals were similarly attained at a lower flow rate and the EF/adsorption process showed higher COD removal efficiencies compared to the EF process. The COD removal efficiency remained stable at approximately76 % and 65 %for flow rates of 25 and 50 $mLmin^{-1}$for the EF system and 92 % and 73 % for flow rates of 25 to 50 $mLmin^{-1}$for the EF/adsorption system, respectively. The TOC removal efficiency at different flow rates was shown in Fig. 10(c). Similarly, TOC removals were higher for the EF/adsorption process when compared to the EF process and increased with decreasing flow rate. TOC removal efficiencies were 61 % and 50 % at a flow rate of 25 $mLmin^{-1}$for EF/adsorption and EF process, respectively.

As can be seen from the results, the colour, COD and TOC removals decreased by increasing the flow rate from 25 to 50 mL min^{-1}. This can be attributed to the decrease of electrochemical treatment time from 60 to 30 min, resulting in less contact time of pollutants with oxidant species produced in the electrochemical reactor. The wastewater flow rate determines the hydraulic retention time (HRT) in the EF reactor. A higher HRT results in higher treatment efficiency and the treatment capacity decreases with a decrease in HRT. Similar results

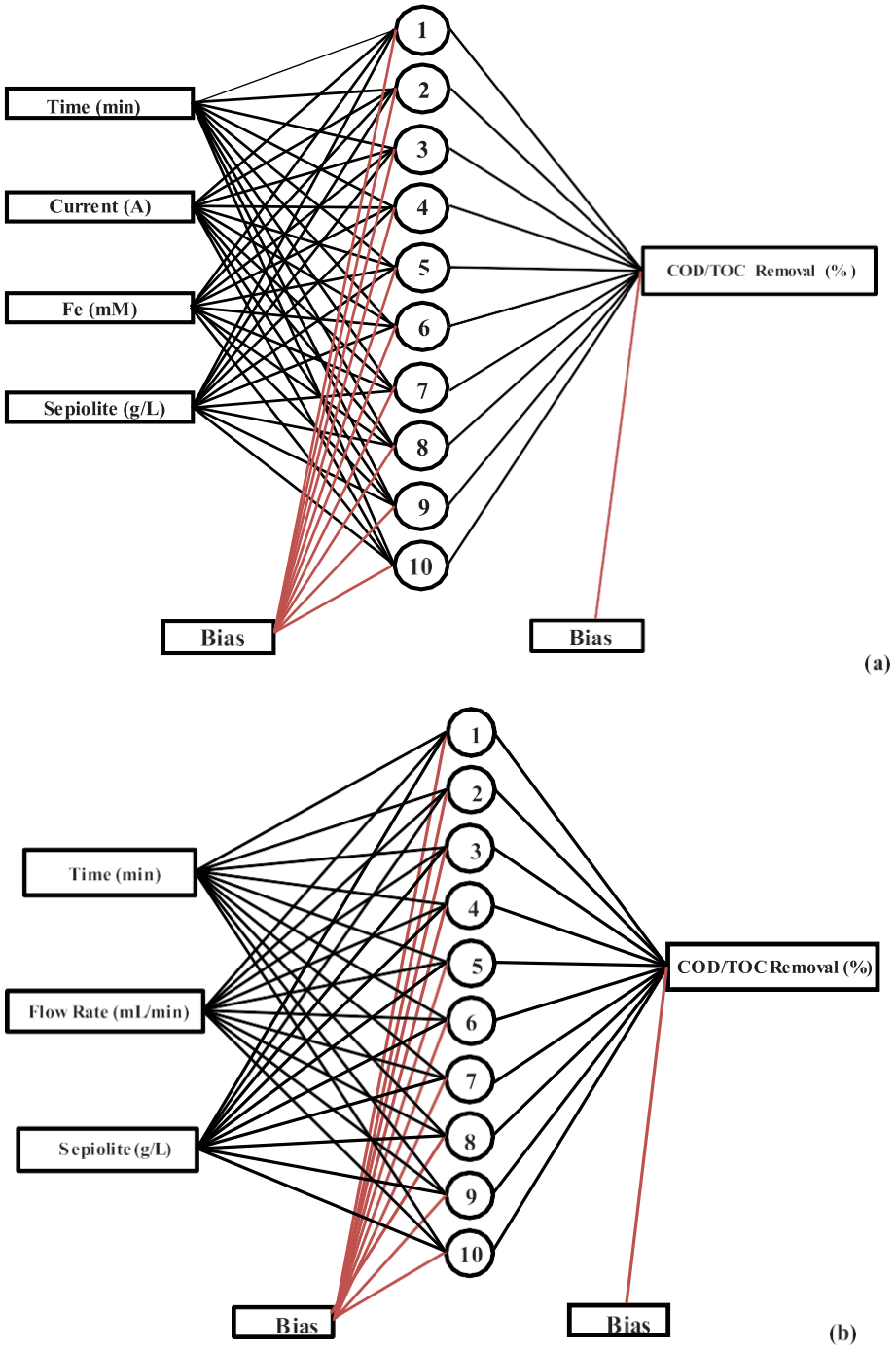

Fig. 12. Schematic structure of ANN used in (a) batch and (b) continuous modes.

were also obtained by Rosales et al. [47] who stated that decolourization of dyes increased with increasing residence time in the continuous EF system. Ren et al. [48] employed a vertical-flow EF reactor for the treatment of tartrazine. They reported that TOC removal increased with decreasing flow rate owing to the increase in HRT. Pajootan et al. [49] also reported that the removal efficiency of AR14 AB92 dyes decreased by increasing the flow rate.

3.6. Evaluation of biodegradability

Average Oxidation State (AOS) and Carbon Oxidation State (COS) parameters were used to evaluate the biodegradability of wastewater after EF and EF/adsorption processes. The AOS is employed to identify the variations causing changes in the biodegradability of wastewater while the COS is considered as the indicator of process efficiency [42].

AOS and COS were calculated as follows:

$$AOS = 4 - 1.5 \times \left(\frac{COD}{\text{þ}}\right) \quad \text{ð16Þ}$$

$$COS = 4 - 1.5 \times \left(\frac{COD}{TOC_0}\right) \quad \text{ð17Þ}$$

where, TOC_0 is the TOC concentration (mg L^{-1}) of textile wastewater. COD and TOC are the COD and TOC concentrations (mg L^{-1}) after the EF process. The values of AOS and COS vary in the range of –4 and + 4

Table 3
Weights matrix for COD removal in batch system, W1: weights between input and hidden layers; W2: weights between hidden and output layers.

Neuron	W1				W2
	Input variables				Output
	Time	Current	Fe	Sepiolite	COD removal %
1	1.35390	−2.60300	1.04500	1.00250	0.16445
2	−0.42929	−2.18450	0.10746	−1.18410	0.38471
3	1.57180	−0.20831	−0.88645	−1.26110	0.18051
4	0.35120	1.74680	−0.97712	0.46749	0.50711
5	−0.19053	0.00718	−1.00420	−1.93300	−0.87638
6	1.00610	−1.86500	0.91216	1.82730	−0.17710
7	0.63769	−2.03090	−1.40130	2.40950	−0.18124
8	−2.34980	−1.45420	0.88926	1.17980	0.11464
9	−0.80673	0.63412	−1.26880	−0.86454	−0.40003
10	1.57880	−1.68870	−0.59601	0.56033	−0.01090

Table 4
Weights matrix for TOC removal in batch system, W1: weights between input and hidden layers; W2: weights between hidden and output layers.

Neuron	W1				W2
	Input variables				Output
	Time	Current	Fe	Sepiolite	TOC removal %
1	0.26482	0.54170	−0.31079	2.65830	0.36391
2	1.24680	0.54847	4.76380	2.53710	0.22346
3	−1.74900	−2.63730	−1.31890	0.54004	−0.01325
4	−5.64160	4.66490	−3.64730	3.77600	−0.05319
5	1.53900	0.03460	1.82900	1.08910	0.23850
6	−3.63800	0.70694	−1.73860	0.61410	−0.03110
7	2.75530	−1.16750	−3.08620	7.61760	−0.08420
8	−0.16674	0.26325	−1.67870	−4.64870	−0.55870
9	−1.91770	−2.28200	−2.27510	−1.70770	0.13072
10	3.51330	0.16942	−2.73040	−2.28150	−0.04881

for methane and carbon dioxide, representing the most reduced and the most oxidized form of carbon [50,51].

The AOS can be employed as an overall measure of the organic compounds remaining in the wastewater, while COS represents the elimination of carbon from the wastewater in the form of CO_2. Fig. 11 shows that AOS and COS parameters have an initial value of −1.89 which indicates the high reduction level of the textile wastewater and increased with the treatment period, reaching a maximum value of 0.38 and 1.52 for EF and 1.78 and 3.12 EF/adsorption processes, respectively. High COS values indicate that the organic compounds in the process effluent comprise mainly of organic acids, and the increase of AOS shows enhancement of biodegradability [42].

3.7. ANN modeling of the EF/adsorption process

Artificial neural network is defined as a computation tool stimulated by biological neural systems. ANN consists of a group of interrelated artificial neurons (nodes), arranged in a variety of layers (input, hidden and output layers). The neurons are connected to each other through synapses which are defined as connections or links [52]. ANNs can be trained to detect trends and reveal the patterns in a complicated system [53].

In this study, the ANN model which contained three layers and topology of 4:10:1 in the batch system and 3:10:1 in the continuous system was used to predict the treatment efficiency of the EF/adsorption process. The structure of the neural network for the batch and continuous system was shown in Fig. 12(a) and (b), respectively.

A series of topologies with a number of neurons varying from 2 to 20 were tested to determine the optimum number of neurons in the hidden layer. Each topology was repeated three times to avoid random correlation as the weights were randomly initialized. The mean square error (MSE) was used as the error function to evaluate the performance of the model. MSE was calculated by the following equation:

Table 5
Relative importance of input variables on the COD and TOC removal efficiency in batch system.

Input variable	Importance % COD	Importance % TOC
Time	13.9 %	10.6 %
Current	11.5 %	6.0 %
Fe	27.6 %	29.9 %
Sepiolite	47.1 %	53.5 %
Total	100 %	100 %

$$MSE = \frac{1}{N}\sum_{i=1}^{i=N}\left(Y_{i,pred} - Y_{i,exp}\right)^2 \quad (18)$$

where N is the number of data points, $Y_{i,pred}$ predicted data by the model, $Y_{i,exp}$ experimental data and i is the index of data [54]. Since the minimum MSE value was reached with 10 neurons, this number of neurons in the hidden layer was used in the modeling process.

The tan-sigmoid transfer function was used as a transfer function in the hidden layer. This is the most widely used transfer function and is defined by the following equation:

$$f(x) = \frac{1}{1 + \exp(-x)} \quad (19)$$

where f(x) is the output of the hidden neuron [53]. Since the transfer function used in the hidden layer is sigmoid, all samples should be scaled into 0.1–0.9. Therefore, any X_i sample from the training, validation and test datasets was scaled to a new A_i value as follows:

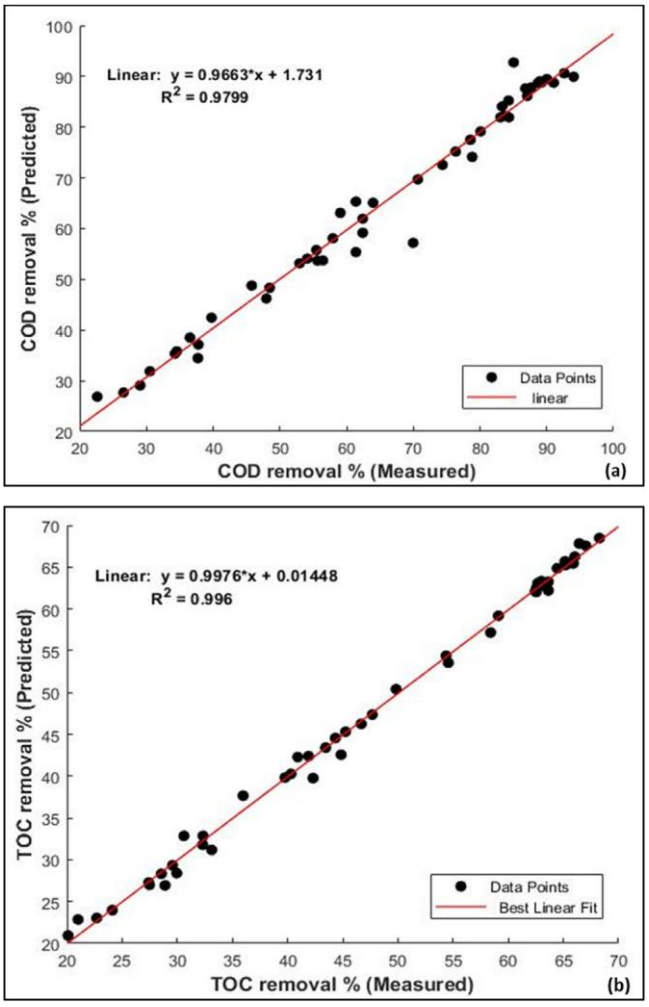

Fig. 13. Comparison between ANN predicted and experimental values of (a) COD and (b) TOC removals in batch system.

$$A \quad 0\,8\,\frac{X_i - min(X_i)}{\max(X_i) - min(X_i)} \quad 0\,1 \qquad \text{þ : 20}$$

where min(X_i) and max(X_i) are minimum and maximum values of X_i variable [55].

The relative importance of the various input variables on the output variables was evaluated by the neural weight matrix. The following equation which is based upon the partition of connecting weights was used:

$$Ij = \frac{\sum_{m=1}^{Nh} |W_{jm}^{ih}| \times |W_{mn}^{ho}|}{\sum_{k=1}^{Ni} \sum_{m=1}^{Nh} |W_{km}^{ih}| \times |W_{mn}^{ho}|} \qquad \text{ð21þ}$$

where I_j is the relative importance of the input variable j^{th} on the output variable, W_s are connection weights, N_i and N_h are the numbers of input and hidden neurons, respectively. The superscripts 'i', 'h' and 'o' indicate the input, hidden and output layers, and subscripts 'k', 'm' and 'n' indicate the input, hidden and output neurons, respectively [56].

Tables 3 and 4 show the weights provided by ANN for COD and TOC removals in the batch system. The neural weight data were used to calculate the effect of each input variable on the output variable. The relative importance of input variables on the COD and TOC removal efficiency in the batch system was shown in Table 5. The obtained results showed that the impact of input variables on the COD and TOC removals was found to be in the following order: sepiolite dose > Fe^{2+} concentration > time > applied current. The relative importance of sepiolite dose, Fe^{2+} concentration, time and applied current on COD and TOC removal efficiency was 47.1 %, 27.6 %, 13.9 % and 11.5 % and 53.5 %, 29.9 %, 10.6 % and 6 %, respectively.

The experimental values were compared with predicted values to assess the accuracy of the ANN model. Fig. 13(a) and (b) show a comparison between the experimental and predicted COD and TOC removals based on a neural network model for the batch system. The plots show correlation coefficients (R^2) of 0.979 for COD removal and 0.996 for TOC removal. The results revealed that the ANN model provided good predictions with high correlation coefficients for COD and TOC removal.

The ANN used in the continuous system provided the weights listed in Tables 6 and 7 for COD and TOC removal. The relative importance of input variables on the COD and TOC removal efficiency obtained by the neural weight matrix in the continuous system was shown in Table 8. It can be seen that all of the parameters (time, flow rate, and sepiolite addition) have strong effects on the COD and TOC removal efficiency. However, time appeared to be the most important parameter in the COD removal with a relative importance of 54.1 %, while flow rate appeared to be the most important parameter in the TOC removal with a relative importance of 52.6 %. Fig. 14(a) and (b) show a comparison between experimental and calculated COD and TOC removals by using a neural network model in the continuous system. Plots in this figure have correlation coefficients of 0.980 and 0.993 for COD and TOC removal, respectively. The correlation coefficients of the plots indicate the reliability of the model. The results confirm that the neural network model reproduces the COD and TOC removals in the batch and continuous system within experimental

Table 6
Weights matrix for COD removal in continuous system, W1: weights between input and hidden layers; W2: weights between hidden and output layers.

Neuron	W1			W2
	Input variables			Output
	Time	Flow Rate	Sepiolite	COD removal %
1	2.90640	−1.43850	−0.15265	0.89757
2	−0.14866	2.70140	1.66920	0.71658
3	0.78649	2.28460	1.50890	0.06533
4	−1.89920	3.37570	0.27420	−1.18690
5	−3.10970	1.43570	−0.60433	0.13602
6	−0.36869	0.30367	−3.54500	0.12968
7	−2.33930	−1.74690	−4.10890	−0.32688
8	−1.28160	−2.59580	2.07380	−0.71802
9	0.17516	−1.51120	−2.64700	0.01343
10	0.51773	1.39830	0.44730	0.71662

Table 7
Weights matrix for TOC removal in continuous system, W1: weights between input and hidden layers; W2: weights between hidden and output layers.

Neuron	W1			W2
	Input variables			Output
	Time	Flow Rate	Sepiolite	TOC removal %
1	1.46520	−1.05400	0.18265	0.20930
2	0.83980	1.69240	2.09730	1.12600
3	−2.39070	2.74650	1.88400	1.40810
4	−2.61750	−2.39150	−0.13519	0.29165
5	−1.90960	3.38950	2.59960	−1.67380
6	0.41697	2.19110	1.20500	0.32253
7	−0.18998	1.85820	−2.26070	−0.39894
8	−0.10862	2.21970	2.03320	0.29352
9	4.09470	−0.44823	1.15670	0.22472
10	−0.90022	3.38600	2.32310	−1.50790

Table 8
Relative importance of input variables on the COD and TOC removal efficiency in continuous system.

Input variable	Importance % COD	Importance %TOC
Time	54.1 %	27.6 %
Flow rate	28.3 %	52.6 %
Sepiolite	17.6 %	19.8 %
Total	100 %	100 %

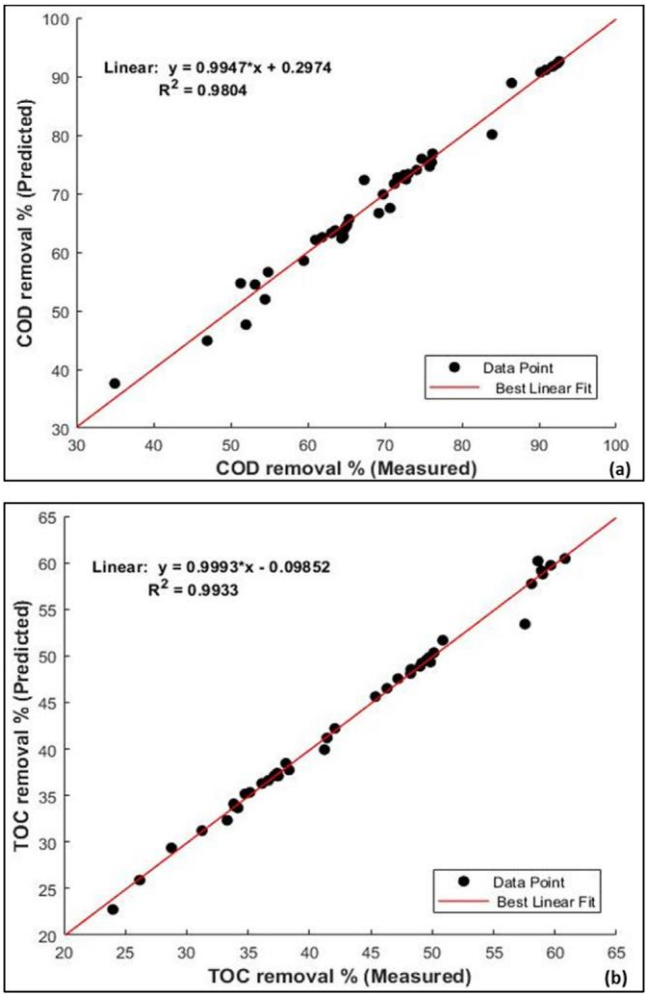

Fig. 14. Comparison between ANN predicted and experimental values of (a) COD and (b) TOC removals in continuous system.

ranges adopted in the established model. Based on the results, it can be concluded that the ANN model can accurately model the experimental data and can be used to predict the output variables under different conditions.

4. Conclusion

Coupling EF and adsorption processes was successfully applied for the remediation of textile industry wastewater. The efficiency of the coupled EF/adsorption system was investigated in both batch and con- tinuous flow modes. Thus, in batch experiments, the effects of reaction time, applied current, Fe^{2+} concentration and sepiolite dose on the process performance were investigated. The optimal operating conditions were found as pH of 3, 1 mM of Fe^{2+}, 0.55 A of current and 5 g/l of sepiolite. The application of the coupled EF/adsorption process resulted in an increase in the degradation efficiency in comparison to the single EF process. Under the optimal operating conditions, 85 % and 58 % COD, 63 % and 36 % TOC removals were attained by the EF/adsorption and the EF processes, respectively. The enhanced removals of COD and TOC were observed owing to the combined effect of adsorption and oxidation reactions. The EF/adsorption coupled system was also operated in a continuous flow mode at different flow rates. It was observed that for the flow rate of 25 mL min^{-1} (the corresponding HRT was 60 min), the colour removal efficiency reached near 90 % and the COD and TOC removal efficiencies were 92 % and 60 %, respectively. Further, the AOS and the COS values increased significantly after the EF/adsorption treatment indicating biodegradability enhancement in the textile industry wastewater. Moreover, in order to predict the COD and the TOC removals by the coupled EF/adsorption and the single EF processes, an Artificial Neural Network model was developed. A good agreement was observed between the experimental results and the theoretical values, indicating that the ANN model can predict the effect of various operating parameters on the removal of the COD and the TOC, with high accuracy. The overall data show that combining the EF and the adsorption processes leads to enhanced efficiencies and sustainability in the textile effluent treatment.

Acknowledgement

This study was conducted in the frame of the ERANET-MED project SETPROpER and financially supported by the Scientific and Technological Research Council of Türkiye (TUBITAK) with the grant number of 115Y845.

References

[1] H. Lei, H. Li, Z. Li, Z. Li, K. Chen, X. Zhang, H. Wang, Electro-Fenton degradation of cationic red X-GRL using an activated carbon fiber cathode, Process Saf. Environ. Prot. 88 (2010) 431–438.
[2] A.K. Verma, R.R. Dash, P. Bhunia, A review on chemical coagulation/flocculation technologies for removal of colour from textile wastewaters, J. Environ. Manage. 93 (2012) 154–168.
[3] M. Ağtas, O. Yılmaz, M. Dilaver, K. Alp, I. Koyuncu, Hot water recovery and reuse in textile sector with pilot scale ceramic ultrafiltration/nanofiltration membrane system, J. Clean. Prod. 256 (2020) 120359.
[4] L.G.M. Silva, F.C. Moreira, M.P. Cechinel, L.P. Mazur, A.A.U. Souza, S.M.A.G.U. Souza, R.A.R. Boaventura, V.J.P. Vilar, Integration of Fenton's reaction based processes and cation exchange processes in textile wastewater treatment as a strategy for water reuse, J. Environ. Manage. 272 (2020) 111082.
[5] S. Samuchiwal, A. Bhattacharya, A. Malik, Treatment of textile effluent using an anaerobic reactor integrated with activated carbon and ultrafiltration unit (AN-ACF-UF process) targeting salt recovery and its reusability potential in the pad-batch process, J. Water Process. Eng. 40 (2021) 101770.
[6] J. Dasgupta, J. Sikder, S. Chakraborty, S. Curcio, E. Drioli, Remediation of textile effluents by membrane based treatment techniques: a state of the art review, J. Environ. Manage. 147 (2015) 55–72.
[7] J. Blanco, F. Torrades, M. Morón, M. Brouta-Agnésa, J. García-Montaño, Photo-Fenton and sequencing batch reactor coupled to photo-Fenton processes for textile wastewater reclamation: feasibility of reuse in dyeing processes, Chem. Eng. J. 240 (2014) 469–475.
[8] H. Zazou, H. Afanga, S. Akhouairi, H. Ouchtak, A. Ait Addi, R. Ait Akbour, A. Assabbane, J. Douch, A. Elmchaouri, J. Duplay, A. Jada, M. Hamdani, Treatment of textile industry wastewater by electrocoagulation coupled with electrochemical advanced oxidation process, J. Water Process. Eng. 28 (2019) 214–221.
[9] Z. Hu, J. Cai, G. Song, Y. Tian, M. Zhou, Anodic oxidation of organic pollutants: anode fabrication, process hybrid and environmental applications, Curr. Opin. Electrochem. 26 (2021) 100659.
[10] C.A. Martínez-Huitle, M. Panizza, Review article electrochemical oxidation of organic pollutants for wastewater treatment, Curr. Opin. Electrochem. 11 (2018) 62–71.
[11] Y. Jiang, H. Zhao, J. Liang, L. Yue, T. Li, Y. Luo, Q. Liu, S. Lu, A.M. Asiri, Z. Gong, X. Sun, Anodic oxidation for the degradation of organic pollutants: anode materials, operating conditions and mechanisms. A mini review, Electrochem. Commun. 123 (2021) 106912.
[12] P.V. Nidheesh, M. Zhou, M.A. Oturan, An overview on the removal of synthetic dyes from water by electrochemical advanced oxidation processes, Chemosphere 197 (2018) 210–227.
[13] I. Sirés, E. Brillas, Upgrading and expanding the electro-Fenton and related processes, Curr. Opin. Electrochem. 27 (2021) 100686.
[14] Z. Deng, C. Ma, S. Yan, K. Dong, Q. Liu, Y. Luo, Y. Liu, J. Du, X. Sun, B. Zheng, One-dimensional conductive metal–organic framework nanorods: a highly selective electrocatalyst for the oxygen reduction to hydrogen peroxide, J. Mater. Chem. A 9 (2021) 20345–20349.
[15] L. Zhang, J. Liang, L. Yue, K. Dong, Z. Xu, T. Li, Q. Liu, Y. Luo, Y. Liu, S. Gao, A.M. Asiri, Q. Kong, X. Guo, X. Sun, CoTe nanoparticle-embedded N-doped hollow carbon polyhedron: an efficient catalyst for H_2O_2 electrosynthesis in acidic media, J. Mater. Chem. A 9 (2021) 21703–21707.
[16] K. Dong, J. Liang, Y. Ren, Y. Wang, Z. Xu, L. Yue, T. Li, Q. Liu, Y. Luo, Y. Liu, S. Gao, M.S. Hamdy, Q. Li, D. Ma, X. Sun, Electrochemical two-electron O_2 reduction reaction toward H_2O_2 production: using cobalt porphyrin decorated carbon nanotubes as a nanohybrid catalyst, J. Mater. Chem. A 9 (2021) 26019–26027.
[17] Z. Xu, J. Liang, Y. Wang, K. Dong, X. Shi, Q. Liu, Y. Luo, T. Li, Y. Jia, A.M. Asiri, Z. Feng, Y. Wang, D. Ma, X. Sun, Enhanced electrochemical H_2O_2 production via two-electron oxygen reduction enabled by surface-derived amorphous oxygen-deficient TiO_2-x, ACS Appl. Mater. Interfaces 13 (28) (2021) 33182–33187.
[18] Q. Chen, C. Ma, S. Yan, J. Liang, K. Dong, Y. Luo, Q. Liu, T. Li, Y. Wang, L. Yue, B. Zheng, Y. Liu, S. Gao, Z. Jiang, W. Li, X. Sun, Greatly facilitated two-electron

electroreduction of oxygen into hydrogen peroxide over TiO_2 by Mn doping, ACS Appl. Mater. Interfaces 13 (39) (2021) 46659–46664.
[19] B. Ramirez-Pereda, A. Álvarez-Gallegos, Y.A. Bustos-Terrones, S. Silva-Martínez, A. Hernández-Pérez, Effective electro-fenton treatment for a real textile effluent: a case study, J. Water Process. Eng. 37 (2020) 101434.
[20] S.O. Ganiyu, M.A. Martínez-Huitle, M.A. Oturan, Electrochemical advanced oxidation processes for wastewater treatment: advances in formation and detection of reactive species and mechanisms, Curr. Opin. Electrochem. 27 (2021) 100678.
[21] J. Casado, Towards industrial implementation of Electro-Fenton and derived technologies for wastewater treatment: a review, J. Environ. Chem. Eng. 7 (2019) 102823.
[22] M.S. Çelebi, N. Oturan, H. Zazou, M. Hamdani, M.A. Oturan, Electrochemical oxidation of carbaryl on platinum and boron-doped diamond anodes using electro- Fenton technology, Sep. Purif. Technol. 156 (2015) 996–1002.
[23] P.V. Nidheesh, R. Gandhimathi, Trends in electro-Fenton process for water and wastewater treatment: an overview, Desalination 299 (2012) 1–15.
[24] M. Alkan, Ö. Demirbas, M. Doğan, Adsorption kinetics and thermodynamics of an anionic dye onto sepiolite, Microporous Mesoporous Mater. 101 (2007) 388–396.
[25] M. Alkan, M. Doğan, Y. Turhan, Ö. Demirbas, P. Turan, Adsorption kinetics and mechanism of maxilon blue 5G dye on sepiolite from aqueous solutions, Chem. Eng. J. 139 (2008) 213–223.
[26] F. Largo, R. Haounati, S. Akhouairi, H. Ouachtak, R. El Haouti, A. El Guerdaoui, N. Hafid, D.M.F. Santos, F. Akbal, A. Kuleyin, A. Jada, A. Ait Addi, Adsorptive removal of both cationic and anionic dyes by using sepiolite clay mineral as adsorbent: experimental and molecular dynamic simulation studies, J. Mol. Liquids 318 (2020) 114247.
[27] E. Rosales, D. Anasie, M. Pazos, J. Lazar, M.A. Sanromán, Kaolinite adsorption- regeneration system for dyestuff treatment by Fenton based processes, Sci. Total Environ. 622–623 (2018) 556–562.
[28] F.E. Titchou, H. Zazou, H. Afanga, J. El Gaayda, R.A. Akbour, P.V. Nidheesh, M. Hamdani, An overview on the elimination of organic contaminants from aqueous systems using electrochemical advanced oxidation processes, J. Water Process. Eng. 41 (2021) 102040.
[29] K. Paździor, L. Bilińska, S. Ledakowicz, A review of the existing and emerging technologies in the combination of AOPs and biological processes in industrial textile wastewater treatment, Chem. Eng. J. 376 (2019) 120597.
[30] M. Panizza, M.A. Oturan, Degradation of Alizarin Red by electro-Fenton process using a graphite-felt cathode, Electrochim. Acta 56 (2011) 7084–7087.
[31] J. Li, D. Song, K. Du, Z. Wang, C. Zhao, Performance of graphite felt as a cathode and anode in the electro-Fenton process, RSC Adv. 9 (2019) 38345.
[32] M. Panizza, G. Cerisola, Electro-Fenton degradation of synthetic dyes, Water Res. 43 (2009) 339–344.
[33] F.E.F. Rego, A.M.S. Solano, I.C.C. Soares, D.R. Silva, C.A.M. Huitle, M. Panizza, Application of electro-Fenton process as alternative for degradation of Novacron Blue dye, J. Environ. Chem. Eng. 2 (2014) 875–880.
[34] H.S. El-Desoky, M.M. Ghoneim, N.M. Zidan, Decolorization and degradation of Ponceau S azo-dye in aqueous solutions by the electrochemical advanced Fenton oxidation, Desalination 264 (2010) 143–150.
[35] H. He, Z. Zhou, Electro-Fenton process for water and wastewater treatment, Critical Review, Environ. Sci. Technol. 47 (2017) 2100–2131.
[36] A. Kuleyin, A. Gök, F. Akbal, Treatment of textile industry wastewater by electro- Fenton process using graphite electrodes in batch and continuous mode, J. Environ. Chem. Eng. 9 (2021) 104782.
[37] C.-T. Wang, W.-L. Chou, M.-H. Chung, Y.-M. Kuo, COD removal from real dyeing wastewater by electro-Fenton technology using an activated carbon fiber cathode, Desalination 253 (2010) 129–134.
[38] I. Khatri, S. Singh, A. Garg, Performance of electro-Fenton process for phenol removal using iron electrodes and activated carbon, J. Environ. Chem. Eng. 6 (2018) 7368–7376.
[39] J. Zou, X. Peng, M. Li, Y. Xiong, B. Wang, F. Dong, B. Wang, Electrochemical oxidation of COD from real textile wastewaters: kinetic study and energy consumption, Chemosphere 171 (2017) 332–338.
[40] R. Bhatnagar, H. Joshi, I.D. Mall, V.C. Srivastava, Electrochemical oxidation of textile industry wastewater by graphite electrodes, J. Environ. Sci. Health, Part A 49 (2014) 955–966.
[41] G.B. Raju, M.T. Karuppiah, S.S. Latha, D.L. Priya, S. Parvathy, S. Prabhakar, Electrochemical pre-treatment of textile effluents and effect of electrode materials on the removal of organics, Desalination 249 (2009) 167–174.
[42] E. GilPavas, S. Correa-Sanchez, Optimization of the heterogeneous electro-Fenton process assisted by scrap zero-valent iron for treating textile wastewater: Assessment of toxicity and biodegradability, J. Water Process. Eng. 32 (2019) 100924.
[43] K. Yong, Y. Jia, W. Zhiliang, Y. Shiping, C. Zhidong, Application of expanded graphite/attapulgite composite materials as electrode for treatment of textile wastewater, Appl. Clay Sci. 46 (2009) 358–362.
[44] H. Afanga, H. Zazou, F.E. Titchou, Y. Rakhila, R. Ait Akbour, A. Elmchaouri, J. Ghanbaja, M. Hamdani, Integrated electrochemical processes for textile industry wastewater treatment: system performances and sludge settling characteristics, Sustain. Environ. Res. 30 (2020) 2.
[45] F. Ghanbari, M. Moradi, A comparative study of electrocoagulation, electrochemical Fenton, electro-Fenton and peroxi-coagulation for decolorization of real textile wastewater: electrical energy consumption and biodegradability improvement, J. Environ. Chem. Eng. 3 (2015) 499–506.

[46] E. GilPavas, J. Medina, I. Dobrosz-Go´mez, M.A. Go´mez-Garci, Statistical optimization of industrial textile wastewater treatment by electrochemical methods, J. Appl. Electrochem. 44 (2014) 1421–1430.
[47] E. Rosales, M. Pazos, M.A. Longo, M.A. Sanromán, Electro-Fenton decoloration of dyes in a continuous reactor: a promising technology in coloured wastewater treatment, Chem. Eng. J. 155 (2009) 62–67.
[48] G. Ren, M. Zhou, M. Liu, L. Ma, H. Yang, A novel vertical-flow electro-Fenton reactor for organic wastewater treatment, Chem. Eng. J.298 (2016) 55–67.
[49] E. Pajootan, M. Arami, M. Rahimdokht, Discoloration of wastewater in a continuous electro-Fenton process using modified graphite electrode with multi-walled carbon nanotubes/surfactant, Sep. Purif. Technol. 130 (2014) 34–44.
[50] M. Ahmadi, F. Ghanbari, S. Madihi-Bidgoli, Photoperoxi-coagulation using activated carbon fiber cathode as an efficient method for benzotriazole removal from aqueous solutions: Modelling, optimization and mechanism, J. Photochem. Photobiol. A 322–323 (2016) 85–94.
[51] S. Jorfi, S. Pourfadakari, M. Ahmadi, Electrokinetic treatment of high saline petrochemical wastewater: evaluation and scale-up, J. Environ. Manage. 204 (2017) 221–229.
[52] M. Radwan, M.G. Alal, H. Eletriby, Optimization and modeling of electro-Fenton process for treatment of phenolic wastewater using nickel and sacrificial stainless steel anodes, J. Water Process. Eng. 22 (2018) 155–162.
[53] A.M. Gholizadeh, M. Zarei, M. Ebratkhahan, A. Hasanzadeh, Phenazopyridine degradation by electro-Fenton process with magnetite nanoparticles-activated carbon cathode, artificial neural networks modelling, J. Environ. Chem. Eng. 9 (2021) 104999.
[54] A. Aleboyeh, M.B. Kasiri, M.E. Olya, H. Aleboyeh, Prediction of azo dye decolorization by UV/H_2O_2 using artificial neural networks, Dyes Pigm. 77 (2008) 288–294.
[55] D. Salari, A. Niaei, A. Khataee, M. Zarei, Electrochemical treatment of dye solution containing C.I. Basic Yellow 2 by the peroxi-coagulation method and modeling of experimental results by artificial neural networks, J. Electroanal. Chem. 629 (2009) 117–125.
[56] E.S. Elmolla, M. Chaudhuri, M.M. Eltoukhy, The use of artificial neural network (ANN) for modelling of COD removal from antibiotic aqueous solution by the Fenton process, J. Hazard. Mater. 179 (2010) 127–134.